

Plasmon polaritons in cubic lattices of spherical metallic nanoparticles

Simon Lamowski,¹ Felicitas Hellbach,¹ Eros Mariani,² Guillaume Weick,^{3,*} and Fabian Pauly^{1,†}

¹*Department of Physics, University of Konstanz, D-78457 Konstanz, Germany*

²*Centre for Graphene Science, Department of Physics and Astronomy,
University of Exeter, Stocker Rd. EX4 4QL Exeter, UK*

³*Institut de Physique et Chimie des Matériaux de Strasbourg,
Université de Strasbourg, CNRS UMR 7504, F-67034 Strasbourg, France*

We investigate theoretically plasmon polaritons in cubic lattices of interacting spherical metallic nanoparticles. Dipolar localized surface plasmons on each nanoparticle couple through the near field dipole-dipole interaction and form collective plasmons which extend over the whole metamaterial. Coupling these collective plasmons in turn to photons leads to plasmon polaritons. We derive within a quantum model general semi-analytical expressions to evaluate both plasmon and plasmon-polariton dispersions that fully account for nonlocal effects in the dielectric function of the metamaterial. Within this model, we discuss the influence of different lattice symmetries and predict related polaritonic gaps within the near-infrared to the visible range of the spectrum that depend on wavevector direction and polarization.

PACS numbers: 73.20.Mf, 71.36.+c, 78.67.Bf, 73.22.Lp

I. INTRODUCTION

Plasmonic metamaterials can be exploited to manipulate light at subwavelength scales and may be used to tailor optical properties [1–3]. They consist of meta-atoms with possibly complicated subwavelength structures that are arranged in a controlled fashion [4]. Potential applications of such metamaterials range from optical cloaking over planar hyperlenses to optical data processing [5, 6].

The study of the optical properties of one-dimensional (1D), two-dimensional (2D) and three-dimensional (3D) arrays of metallic particles is an active field of research [7]. In the past mostly 1D and 2D systems were investigated both in theory and experiment [3, 4], since they are much easier to fabricate reliably with established techniques than 3D arrays. Due to the advances in nanofabrication, agreement between simulations and measurements in 1D and 2D regarding predicted plasmonic properties is nowadays obtained quite routinely [7]. It is of current interest to also understand systematically the structure-property relationships in 3D crystalline arrangements of meta-atoms where, beside the shape and the size of the nanoparticle itself, the spacing and the crystal symmetry can be controlled independently. Indeed, the development of reliable techniques to control 3D assemblies of plasmonic nanoparticles is presently a very active research area, and such a goal can now be achieved by using surface ligands or DNA templates [7–10].

Many of the optical properties of 1D, 2D, and 3D plasmonic metamaterials based on metallic nanoparticles can be understood in terms of classical electrodynamics [2, 7]. Depending on the distance between the meta-atoms, two qualitatively different regimes emerge [4]. In the first regime, the distance between the meta-atoms is of the order of the wavelength associated with the plasmonic resonance, so that

diffractive far-field interactions between the meta-atoms of the array constructively interfere, leading to collective modes termed surface lattice resonances. In the second, opposite regime, the meta-atom separation is much smaller than the resonance wavelength so that near-field interactions become predominant, leading to collective plasmons that are extended over the whole metamaterial. We concentrate in the present paper on the latter regime.

Early studies on the plasmonic properties of near-field-coupled metallic nanoparticles focused on one-dimensional chains using a nonretarded model of point dipoles [11–14], followed by fully-retarded approaches [15–21]. Three-dimensional metastructures were also investigated using more approximate approaches such as the Maxwell-Garnett effective medium theory [7]. In addition to the classical treatments, a quantum approach was recently applied to 1D [22], 2D [23, 24] and 3D systems [25] that is capable of taking nonlocal effects in the dielectric function into account.

In this work, we study the less explored 3D plasmonic arrays in the regime of near-field coupling between spherical metallic nanoparticles. In contrast to 1D and 2D, a strong coupling between light and the plasmonic excitations of the nanoparticles is expected in 3D. Indeed, as pointed out by Hopfield in the context of exciton polaritons [26], the semiclassical theory of radiation is inadequate for describing the optical properties of the metamaterial due to the lattice translational symmetry of the system. For this reason, we use an analytically tractable quantum model to describe the strong interaction between plasmons and light and take also the nonlocal effects in the dielectric function into account. We consider small particle sizes of some 10 nm in radius, where the particles are polarized completely by light and the response is dipolar in nature. In this regime, quantum-size effects in the optical response of the nanoparticles can be significant [6], and we model the localized surface plasmon (LSP) on each particle as a quantized harmonic oscillator with a corresponding frequency lying in the near-infrared or visible range of the spectrum. Since we consider interparticle distances to be much smaller than the wavelength associated with the dipolar

* guillaume.weick@ipcms.unistra.fr

† fabian.pauly@uni-konstanz.de

LSPs, the latter are coupled to each other through the quasi-static dipole-dipole interaction, disregarding thus retardation effects. Additionally, the LSPs interact with the photons of the quantized light field. The coupled LSPs yield collective plasmons which are extended over the whole metamaterial. These in turn hybridize with photons due to the strong light-matter interaction to form plasmon polaritons.

Our treatment is based on a previous work [25], which we extend here in several ways. We exploit the spherical symmetry of the nanoparticles to produce LSPs on each particle with a natural frequency which is independent of the polarization direction. Furthermore, we study face-centered (fcc) and body-centered (bcc) structures in addition to the simple cubic (sc) structure. Overall, we show that these three highly symmetric systems can exhibit polarization-dependent optical properties such as a band gap in the near-infrared or visible range of the spectrum. Additionally, our systems present polaritonic states with vanishing group velocities, paving the way to metamaterials based on metallic nanoparticles that are able to stop light. Our quantum model is generally applicable to any periodic structure of metallic nanoparticles which is strongly coupled to light.

The paper is organized as follows: In Sec. II we describe our theoretical model to study plasmon polaritons. The general solution to this model is subsequently presented in Sec. III A. The resulting dispersion relations of the collective plasmons and plasmon polaritons for sc, fcc and bcc lattices are presented in Sec. III B and III C, respectively. We finally summarize our results in Sec. IV.

II. MODEL

We consider sc, fcc, or bcc lattices of spherical metallic nanoparticles separated by a center-to-center distance a , as depicted in Fig. 1(a)-(c). The corresponding first Brillouin zones are shown in Fig. 1(d)-(f). Each nanoparticle in the lattice supports three degenerate dipolar LSPs polarized in the x , y or z direction that interact with their neighbors through the quasistatic dipole-dipole interaction [12]

$$V_{\text{dip}}(\mathbf{R}, \mathbf{R}') = \frac{\mathbf{p} \cdot \mathbf{p}' - 3(\mathbf{p} \cdot \hat{n})(\mathbf{p}' \cdot \hat{n})}{4\pi\epsilon_0|\mathbf{R} - \mathbf{R}'|^3}, \quad (1)$$

where \mathbf{p} and \mathbf{p}' are, respectively, the dipole moments associated with the LSPs supported by the nanoparticles located at the lattice sites \mathbf{R} and \mathbf{R}' , $\hat{n} = (\mathbf{R} - \mathbf{R}')/|\mathbf{R} - \mathbf{R}'|$, and ϵ_0 is the vacuum permittivity. Here and in what follows, the hats denote unit vectors. The quasistatic approximation above is valid for center-to-center interparticle distances ρ in the range $3r \lesssim \rho \ll q_0^{-1}$ [14], with r the nanoparticle radius and $q_0 = \omega_0/c$ the wavenumber associated with the LSP resonance frequency ω_0 (which typically lies in the near-infrared to visible range of the spectrum), with c the speed of light in vacuum.

The LSPs on each nanoparticle interact with photonic modes, hence forming plasmon polaritons. These photonic modes have a band structure which follows from the translational symmetry of the lattice, with dispersion $c|\mathbf{q} + \mathbf{K}|$. Here,

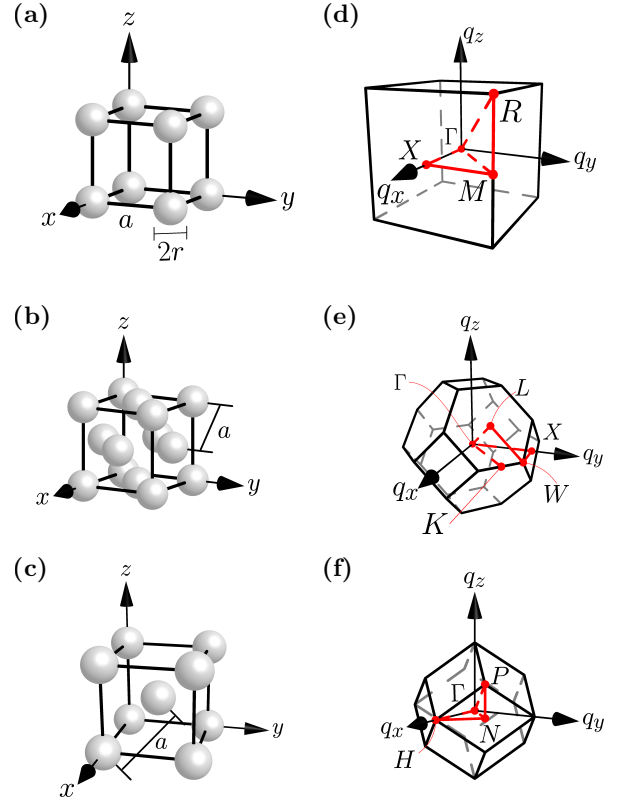


FIG. 1. (Color online) Conventional cells for (a) sc, (b) fcc, and (c) bcc lattices of spherical metallic nanoparticles of radius r , with a the primitive lattice parameter. (d)-(f) Corresponding first Brillouin zones, where the red lines indicate the paths over which the plasmon dispersions are plotted in Fig. 2.

\mathbf{q} is the photon momentum in the first Brillouin zone, and \mathbf{K} is a vector of the reciprocal lattice. Photons with $\mathbf{K} \neq 0$ have an energy which is much higher than the LSP resonance frequency ω_0 , so that they do not significantly couple to the plasmons. In the remainder of this paper, we thus only consider photons belonging to the first branch with $\mathbf{K} = 0$ and their coupling to collective plasmons.

We write the full Hamiltonian of the system as

$$H = H_{\text{pl}} + H_{\text{ph}} + H_{\text{pl-ph}}, \quad (2)$$

where H_{pl} and H_{ph} denote the plasmonic and photonic Hamiltonians, respectively, and where $H_{\text{pl-ph}}$ is the interaction Hamiltonian between both subsystems. The purely plasmonic part reads [23–25]

$$H_{\text{pl}} = \hbar\omega_0 \sum_{\mathbf{q}, \hat{\sigma}} b_{\mathbf{q}}^{\dagger} b_{\mathbf{q}}^{\hat{\sigma}} + \hbar\Omega \sum_{\mathbf{q}, \hat{\sigma}, \hat{\sigma}'} f_{\mathbf{q}}^{\hat{\sigma}\hat{\sigma}'} \left[b_{\mathbf{q}}^{\dagger} \left(b_{\mathbf{q}}^{\hat{\sigma}'} + b_{-\mathbf{q}}^{\hat{\sigma}'\dagger} \right) + \text{h.c.} \right], \quad (3)$$

with

$$f_{\mathbf{q}}^{\hat{\sigma}\hat{\sigma}'} = \sum_{\rho} \left(\frac{a}{\rho} \right)^3 \frac{\cos(\mathbf{q} \cdot \boldsymbol{\rho})}{2} [\delta_{\hat{\sigma}\hat{\sigma}'} - 3(\hat{\sigma} \cdot \hat{\rho})(\hat{\sigma}' \cdot \hat{\rho})]. \quad (4)$$

In Eq. (3), $b_{\mathbf{q}}^{\hat{\sigma}\dagger}$ and $b_{\mathbf{q}}^{\hat{\sigma}}$, respectively, create and annihilate an LSP with momentum \mathbf{q} and polarization $\hat{\sigma} = \hat{x}, \hat{y}$ or \hat{z} . The first term on the right-hand side of Eq. (3) describes the uncoupled LSPs, while the second one with coupling constant $\Omega = (\omega_0/2)(r/a)^3$ corresponds to the quasistatic dipole-dipole interaction (1) between nanoparticles linked by the vector $\boldsymbol{\rho}$ up to a cutoff distance ρ_c . Within our quasistatic approximation, the latter quantity has a maximal allowed value of the order of q_0^{-1} , so that, unless otherwise stated, we set $\rho_c = q_0^{-1}$ in the remainder of this paper.

In Eq. (2), the photonic subsystem is described by

$$H_{\text{ph}} = \sum_{\mathbf{q}, \hat{\lambda}_{\mathbf{q}}} \hbar \omega_{\text{ph}, \mathbf{q}} c_{\mathbf{q}}^{\hat{\lambda}_{\mathbf{q}}\dagger} c_{\mathbf{q}}^{\hat{\lambda}_{\mathbf{q}}}, \quad (5)$$

where $c_{\mathbf{q}}^{\hat{\lambda}_{\mathbf{q}}}$ annihilates and $c_{\mathbf{q}}^{\hat{\lambda}_{\mathbf{q}}\dagger}$ creates a photon with momentum \mathbf{q} , dispersion $\omega_{\text{ph}, \mathbf{q}} = c|\mathbf{q}|$, and transverse polarization $\hat{\lambda}_{\mathbf{q}}$ (i.e., $\hat{\lambda}_{\mathbf{q}} \cdot \hat{q} = 0$). Within the dipolar approximation, the light-matter interaction appearing in Eq. (2) takes the form

$$H_{\text{pl-ph}} = i \hbar \omega_0 \sum_{\mathbf{q}, \hat{\sigma}, \hat{\lambda}_{\mathbf{q}}} \hat{\sigma} \cdot \hat{\lambda}_{\mathbf{q}} \xi_{\mathbf{q}} \left(b_{\mathbf{q}}^{\hat{\sigma}\dagger} c_{\mathbf{q}}^{\hat{\lambda}_{\mathbf{q}}} + b_{\mathbf{q}}^{\hat{\sigma}} c_{-\mathbf{q}}^{\hat{\lambda}_{\mathbf{q}}\dagger} - \text{h.c.} \right) + \hbar \omega_0 \sum_{\mathbf{q}, \hat{\lambda}_{\mathbf{q}}} \xi_{\mathbf{q}}^2 \left(c_{\mathbf{q}}^{\hat{\lambda}_{\mathbf{q}}\dagger} c_{\mathbf{q}}^{\hat{\lambda}_{\mathbf{q}}} + c_{\mathbf{q}}^{\hat{\lambda}_{\mathbf{q}}} c_{-\mathbf{q}}^{\hat{\lambda}_{\mathbf{q}}\dagger} + \text{h.c.} \right), \quad (6)$$

where $\xi_{\mathbf{q}} = (2\Omega\pi/\nu\omega_{\text{ph}, \mathbf{q}})^{1/2}$ contains the structure factor ν which accounts for the different volumes of the primitive cells.

$$\begin{pmatrix} \omega_0 \mathbb{1}_3 + 2\Omega F_{\mathbf{q}} & -2\Omega F_{\mathbf{q}} & -i\omega_0 \xi_{\mathbf{q}} P_{\mathbf{q}} \\ 2\Omega F_{\mathbf{q}} & -(\omega_0 \mathbb{1}_3 + 2\Omega F_{\mathbf{q}}) & i\omega_0 \xi_{\mathbf{q}} P_{\mathbf{q}} \\ i\omega_0 \xi_{\mathbf{q}} P_{\mathbf{q}}^\top & i\omega_0 \xi_{\mathbf{q}} P_{\mathbf{q}}^\top & (\omega_{\text{ph}, \mathbf{q}} + 2\omega_0 \xi_{\mathbf{q}}^2) \mathbb{1}_2 \\ i\omega_0 \xi_{\mathbf{q}} P_{\mathbf{q}}^\top & i\omega_0 \xi_{\mathbf{q}} P_{\mathbf{q}}^\top & 2\omega_0 \xi_{\mathbf{q}}^2 \mathbb{1}_2 \end{pmatrix} \begin{pmatrix} i\omega_0 \xi_{\mathbf{q}} P_{\mathbf{q}} \\ -i\omega_0 \xi_{\mathbf{q}} P_{\mathbf{q}} \\ -2\omega_0 \xi_{\mathbf{q}}^2 \mathbb{1}_2 \\ -(\omega_{\text{ph}, \mathbf{q}} + 2\omega_0 \xi_{\mathbf{q}}^2) \mathbb{1}_2 \end{pmatrix} \begin{pmatrix} \mathbf{u}_{\mathbf{q}}^{\hat{\tau}_{\mathbf{q}}} \\ \mathbf{v}_{\mathbf{q}}^{\hat{\tau}_{\mathbf{q}}} \\ \mathbf{m}_{\mathbf{q}}^{\hat{\tau}_{\mathbf{q}}} \\ \mathbf{n}_{\mathbf{q}}^{\hat{\tau}_{\mathbf{q}}} \end{pmatrix} = \omega_{\text{pp}, \mathbf{q}}^{\hat{\tau}_{\mathbf{q}}} \begin{pmatrix} \mathbf{u}_{\mathbf{q}}^{\hat{\tau}_{\mathbf{q}}} \\ \mathbf{v}_{\mathbf{q}}^{\hat{\tau}_{\mathbf{q}}} \\ \mathbf{m}_{\mathbf{q}}^{\hat{\tau}_{\mathbf{q}}} \\ \mathbf{n}_{\mathbf{q}}^{\hat{\tau}_{\mathbf{q}}} \end{pmatrix}, \quad (9)$$

where the vectors $\mathbf{u}_{\mathbf{q}}^{\hat{\tau}_{\mathbf{q}}}$, $\mathbf{v}_{\mathbf{q}}^{\hat{\tau}_{\mathbf{q}}}$, $\mathbf{m}_{\mathbf{q}}^{\hat{\tau}_{\mathbf{q}}}$, and $\mathbf{n}_{\mathbf{q}}^{\hat{\tau}_{\mathbf{q}}}$ consist of $u_{\mathbf{q}}^{\hat{\tau}_{\mathbf{q}}\hat{\sigma}}$, $v_{\mathbf{q}}^{\hat{\tau}_{\mathbf{q}}\hat{\sigma}}$, $m_{\mathbf{q}}^{\hat{\tau}_{\mathbf{q}}\hat{\lambda}_{\mathbf{q}}}$, and $n_{\mathbf{q}}^{\hat{\tau}_{\mathbf{q}}\hat{\lambda}_{\mathbf{q}}}$, respectively. In Eq. (9), $\mathbb{1}_n$ stands for the $n \times n$ identity matrix, the 3×3 symmetric matrix $F_{\mathbf{q}}$ is defined by its elements $f_{\hat{\sigma}\hat{\sigma}'}$ given in Eq. (4), while the 3×2 matrix $P_{\mathbf{q}}$ is defined as

$$P_{\mathbf{q}} = \begin{pmatrix} \hat{x} \cdot \hat{\lambda}_{1, \mathbf{q}} & \hat{x} \cdot \hat{\lambda}_{2, \mathbf{q}} \\ \hat{y} \cdot \hat{\lambda}_{1, \mathbf{q}} & \hat{y} \cdot \hat{\lambda}_{2, \mathbf{q}} \\ \hat{z} \cdot \hat{\lambda}_{1, \mathbf{q}} & \hat{z} \cdot \hat{\lambda}_{2, \mathbf{q}} \end{pmatrix}, \quad (10)$$

and $P_{\mathbf{q}}^\top$ represents its transpose. Here, the two photon polarizations can be parametrized, e.g., as $\hat{\lambda}_{1, \mathbf{q}} = \hat{z} \times \hat{q}/|\hat{z} \times \hat{q}|$ and $\hat{\lambda}_{2, \mathbf{q}} = \hat{q} \times \hat{\lambda}_{1, \mathbf{q}}/|\hat{q} \times \hat{\lambda}_{1, \mathbf{q}}|$ for $\hat{q} \nparallel \hat{z}$, while for $\hat{q} = \hat{z}$, we choose $\lambda_{1, \mathbf{q}} = \hat{x}$ and $\lambda_{2, \mathbf{q}} = \hat{y}$.

For the sc, fcc, and bcc lattices, the structure factor equals 1, $2^{-1/2} \simeq 0.71$, and $4/3^{3/2} \simeq 0.77$, respectively.

III. RESULTS

A. General solution

The full Hamiltonian (2), representing collective plasmons strongly coupled to photons, can be diagonalized by introducing the bosonic operator

$$\gamma_{\mathbf{q}}^{\hat{\tau}_{\mathbf{q}}} = \sum_{\hat{\sigma}} \left(u_{\mathbf{q}}^{\hat{\tau}_{\mathbf{q}}\hat{\sigma}} b_{\mathbf{q}}^{\hat{\sigma}} + v_{\mathbf{q}}^{\hat{\tau}_{\mathbf{q}}\hat{\sigma}} b_{-\mathbf{q}}^{\hat{\sigma}\dagger} \right) + \sum_{\hat{\lambda}_{\mathbf{q}}} \left(m_{\mathbf{q}}^{\hat{\tau}_{\mathbf{q}}\hat{\lambda}_{\mathbf{q}}} c_{\mathbf{q}}^{\hat{\lambda}_{\mathbf{q}}} + n_{\mathbf{q}}^{\hat{\tau}_{\mathbf{q}}\hat{\lambda}_{\mathbf{q}}} c_{-\mathbf{q}}^{\hat{\lambda}_{\mathbf{q}}\dagger} \right) \quad (7)$$

which annihilates a plasmon polariton with momentum \mathbf{q} and polarization $\hat{\tau}_{\mathbf{q}}$, the latter being generally not aligned along the $\hat{\sigma}$ -axis. Imposing that the operator (7) and its adjoint diagonalize the Hamiltonian (2) as

$$H = \sum_{\mathbf{q}, \hat{\tau}_{\mathbf{q}}} \hbar \omega_{\text{pp}, \mathbf{q}}^{\hat{\tau}_{\mathbf{q}}} \gamma_{\mathbf{q}}^{\hat{\tau}_{\mathbf{q}}\dagger} \gamma_{\mathbf{q}}^{\hat{\tau}_{\mathbf{q}}}, \quad (8)$$

the Heisenberg equation of motion $[\gamma_{\mathbf{q}}^{\hat{\tau}_{\mathbf{q}}}, H] = \hbar \omega_{\text{pp}, \mathbf{q}}^{\hat{\tau}_{\mathbf{q}}} \gamma_{\mathbf{q}}^{\hat{\tau}_{\mathbf{q}}}$ leads to the 10×10 eigensystem

B. Collective plasmons

Before considering in Sec. III C the fully coupled system, it is instructive to first analyze in detail the purely plasmonic problem described by H_{pl} in Eq. (3). Setting $\xi_{\mathbf{q}} = 0$, the matrix defined in Eq. (9) becomes block-diagonal. The lower 4×4 block is diagonal and corresponds to the two degenerate photon branches with dispersion $\omega_{\text{ph}, \mathbf{q}}$. The three positive eigenvalues of the upper 6×6 block yield the collective plasmon dispersion $\omega_{\text{pl}, \mathbf{q}}^{\hat{\tau}_{\mathbf{q}}}$, which is represented in Fig. 2 as a function of momentum \mathbf{q} along the red paths given in Figs. 1(d)-(f) for the sc [Fig. 2(a)], fcc [Fig. 2(b)], and bcc [Fig. 2(c)] lattices. In the figure, we choose an interparticle distance $a = 3r$ and a cutoff radius $\rho_c = 5a/2$, corresponding to a typical LSP resonance frequency $\omega_0 = 2.6 \text{ eV}/\hbar$ and nanoparticle radius $r = 10 \text{ nm}$. This choice of ρ_c includes six shells of nearest neighbors for the three cubic lattices. In Fig. 2, we also show with the help of a color code the collective plasmon

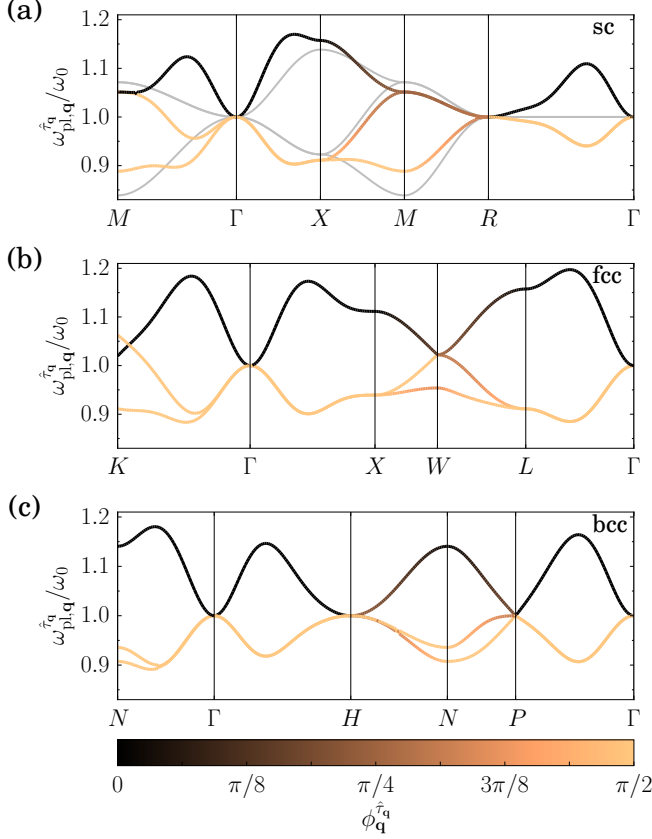


FIG. 2. (Color online) Collective plasmon dispersion $\omega_{\text{pl},\mathbf{q}}^{\hat{\tau}_{\mathbf{q}}}$ in units of the localized surface plasmon frequency ω_0 along the paths shown in red in Fig. 1(d)-(f) for the (a) sc, (b) fcc, and (c) bcc lattices. The color code corresponds to the collective plasmon polarization angle $\phi_{\text{pl},\mathbf{q}}^{\hat{\tau}_{\mathbf{q}}}$, which equals 0 ($\pi/2$) for purely longitudinal (transverse) plasmons. In the figure, the interparticle distance $a = 3r$ and the cutoff radius $\rho_c = 5a/2$ (corresponding to six shells of nearest neighbors) and $\rho_c = a$ [corresponding to nearest neighbors only, cf. Eq. (12)] for the colored thick and gray thin lines, respectively.

polarization angle $\phi_{\hat{\tau}_{\mathbf{q}}}^{\hat{\tau}_{\mathbf{q}}} = \arccos(|\hat{\tau}_{\mathbf{q}} \cdot \hat{q}|)$, where we choose $\hat{\tau}_{\mathbf{q}} = \hat{u}_{\mathbf{q}}^{\hat{\tau}_{\mathbf{q}}}$. Notice that the alternative choice $\hat{\tau}_{\mathbf{q}} = \hat{v}_{\mathbf{q}}^{\hat{\tau}_{\mathbf{q}}}$ leads to the same polarization angle, as the vectors $\mathbf{u}_{\mathbf{q}}^{\hat{\tau}_{\mathbf{q}}}$ and $\mathbf{v}_{\mathbf{q}}^{\hat{\tau}_{\mathbf{q}}}$ are proportional for a given momentum \mathbf{q} . With the above definition of $\phi_{\hat{\tau}_{\mathbf{q}}}^{\hat{\tau}_{\mathbf{q}}}$, longitudinal collective plasmons, which do not couple to light, have a polarization $\phi_{\hat{\tau}_{\mathbf{q}}}^{\hat{\tau}_{\mathbf{q}}} = 0$ (black lines in Fig. 2) while purely transverse modes have a corresponding $\phi_{\hat{\tau}_{\mathbf{q}}}^{\hat{\tau}_{\mathbf{q}}} = \pi/2$ (yellow lines in the figure).

Our results in Fig. 2 indicate that there are two purely transverse collective plasmons and one purely longitudinal one along the high-symmetry axes in the first Brillouin zone [i.e., axes with 2- to 4-fold rotational symmetry, see Figs. 1(d)-(f)]. For less symmetric axes, the collective modes can be of a mixed type [see, e.g., the XM line in Fig. 2(a)]. Moreover, along 3- and 4-fold symmetry axes, the two transverse modes are degenerate (i.e., along ΓR and ΓX for the sc lattice, along

ΓL and ΓX for the fcc lattice, and along ΓP and ΓH for the bcc lattice). This is a manifestation of Neumann's principle [27]: For the collective plasmon dispersion this enforces the degeneracy of the transverse modes for the 3- and 4-fold symmetry lines. The latter degeneracy is lifted for wavevectors with lower symmetry. We also notice that at the Γ point, the matrix $F_{\mathbf{q}} = 0$ [see Eq. (4)] so that $\omega_{\text{pl},\mathbf{q}}^{\hat{\tau}_{\mathbf{q}}} = \omega_0$.

Before we move on to the discussion of the fully coupled system described by the Hamiltonian (2), a comment is in order about the importance of the dipole-dipole interaction beyond nearest neighbors for the collective plasmon dispersion. In Fig. 2(a) we represent by thin gray lines the plasmon dispersion of the sc lattice including nearest neighbors only. In this special case, the matrix $F_{\mathbf{q}}$ is diagonal and its elements read

$$f_{\mathbf{q}}^{\hat{\sigma}\hat{\sigma}'} = \delta_{\hat{\sigma}\hat{\sigma}'} \sum_{\hat{\sigma}''=\hat{x},\hat{y},\hat{z}} (1 - 3\delta_{\hat{\sigma}\hat{\sigma}''}) \cos(a\hat{\sigma}'' \cdot \mathbf{q}). \quad (11)$$

The plasmonic Hamiltonian (3) is therefore separable in \hat{x} , \hat{y} and \hat{z} directions and can be diagonalized analytically, yielding

$$\omega_{\text{pl},\mathbf{q}}^{\hat{\sigma}} = \omega_0 \sqrt{1 + 4 \frac{\Omega}{\omega_0} f_{\mathbf{q}}^{\hat{\sigma}\hat{\sigma}}}. \quad (12)$$

This result [and the corresponding coefficients of the Bogoliubov transformation (7), which we do not report explicitly here] coincide with those found in Ref. [25] for LSP polarizations along \hat{x} , \hat{y} or \hat{z} . As can be seen in Fig. 2(a), including the dipole-dipole interactions beyond those between nearest neighbors can have a qualitative effect as it lifts the degeneracy between plasmon branches, e.g., along the ΓM and ΓR directions. In other regions of the first Brillouin zone, the difference between the dispersions is less significant.

C. Plasmon polaritons

We now consider the fully coupled system represented by the eigensystem (9) and numerically solve for its five positive eigenvalues yielding the plasmon polariton spectrum $\omega_{\text{pp},\mathbf{q}}^{\hat{\tau}_{\mathbf{q}}}$. The latter is shown by solid lines in Fig. 3 for the sc [Figs. 3(a)-(c)], fcc [Figs. 3(d)-(f)], and bcc lattices [Figs. 3(g)-(i)] along 2-fold [Figs. 3(a),(d),(g)], 3-fold [Figs. 3(b),(e),(h)], and 4-fold symmetry axes [Figs. 3(c),(f),(i)], cf. Figs. 1(d)-(f). Along the high-symmetry axes of the first Brillouin zone shown in Fig. 3, the five modes split up into four polaritonic branches (colored solid lines) and one purely longitudinal collective plasmon which does not couple to transverse photons (black lines in the figure, see also Fig. 2). The four polaritonic modes result from the coupling of transverse collective plasmons (see Fig. 2) to photons (whose dispersion relation is shown by dashed lines in Fig. 3).

As can be inferred from Fig. 3, there are two high-energy polaritonic branches (orange solid lines) and two low-energy ones (green solid lines). The two high-energy branches are nearly degenerate and almost do not depend on the choice of the cutoff distance ρ_c . The low-energy polaritonic branches, shown by green solid lines in Fig. 3, have the same degeneracy

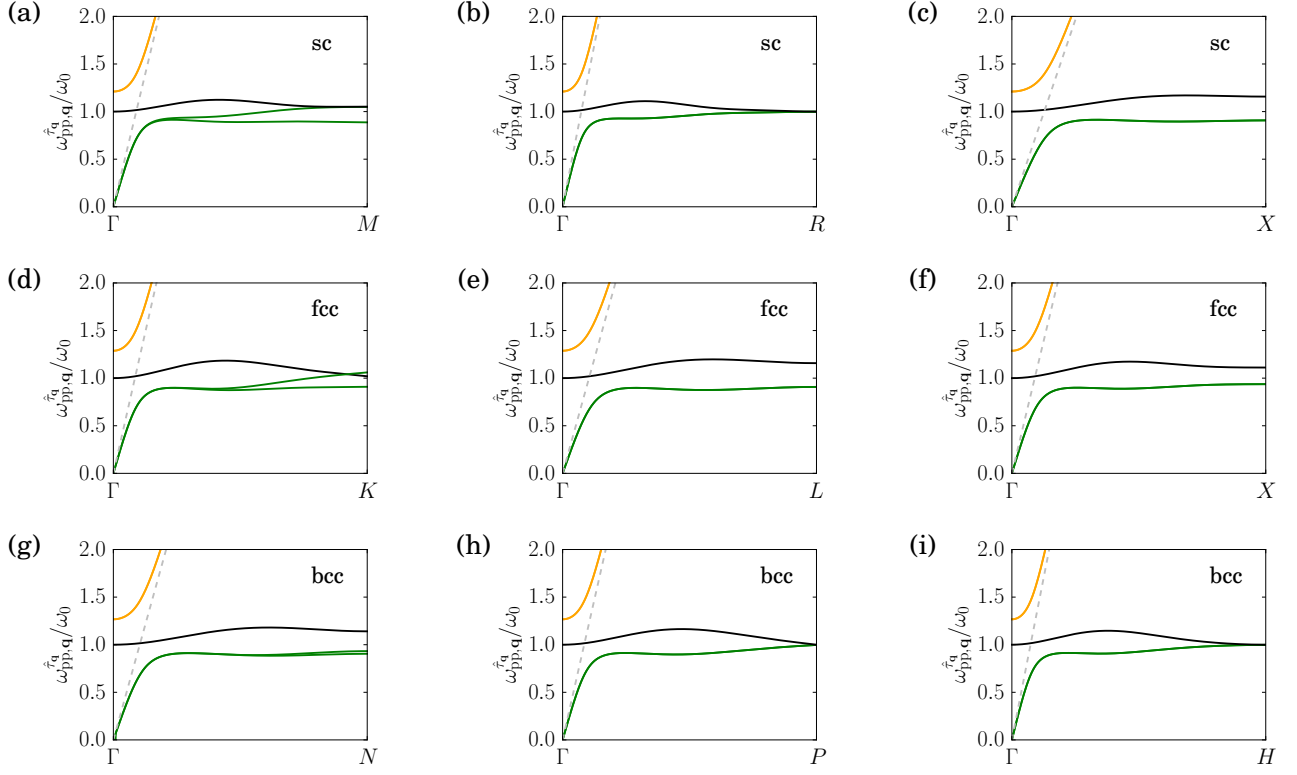


FIG. 3. (Color online) Solid lines: plasmon polariton dispersion relation $\omega_{pp,q}^{\tau}$ in units of the localized surface plasmon frequency ω_0 for the (a)-(c) sc, (d)-(f) fcc, and (g)-(i) bcc lattices along the (a),(d),(g) 2-fold, (b),(e),(h) 3-fold, and (c),(f),(i) 4-fold symmetry axes shown in Fig. 1. Dashed gray lines: free photon dispersion $\omega_{ph,q}$. The parameters in the figure are $a = 3r$ and $\rho_c = q_0^{-1} = 5a/2$.

as the collective plasmon dispersion (compare with Fig. 2) and the light-matter interaction does not lift this degeneracy.

For wavenumbers close to the edge of the first Brillouin zone, the high-energy polaritonic branches (orange solid lines in Fig. 3) asymptotically approach the light cone, while the low-energy ones (green solid lines in the figure) tend to the collective plasmon dispersion. For $\mathbf{q} \rightarrow 0$ (i.e., close to the Γ point), the states corresponding to the low-energy branches are mostly photon-like, with a renormalized group velocity which is smaller than c , indicating an effective index of refraction larger than one. However, the high-energy branches do not tend to ω_0 when $\mathbf{q} \rightarrow 0$. This is due to the strong coupling between collective plasmons and photons [cf. Eq. (6)] which results in a gap between the low- and high-energy polaritonic branches. This polaritonic gap Δ is of the order of 25 % of the LSP resonance frequency ω_0 . For noble-metal nanoparticles, the latter typically lies in the optical range ($\omega_0 \simeq 2\text{--}3\text{ eV}/\hbar$), resulting in a gap of about $\Delta \simeq 0.5\text{--}0.75\text{ eV}/\hbar$. Notice that this estimate is only weakly-dependent on the choice of the cutoff distance ρ_c . The gap in the polaritonic dispersion has important experimental consequences for the optical properties of the metamaterial. Indeed, no plasmon polariton can propagate for frequencies within the bandgap, so that the reflectivity of the metacrystal should be perfect. Moreover, the polaritonic gap depends on the polarization along the

two-fold symmetry axis for the three cubic lattices [see Figs. 3(a),(d),(g)]. This birefringence is directly related to the polarization dependence of the collective plasmon dispersion, the latter being due to the anisotropic nature of the dipole-dipole interaction between the nanoparticles composing the metamaterial. The modulation of the gap can be rather significant for the sc and fcc lattices (of the order of 15 % of ω_0), while for the bcc lattice, the modulation is only very small (only 2 % of ω_0).

We also observe in Fig. 3 several special points for which the derivative of the dispersion relation with respect to the momentum in the directions shown in the figure vanishes [see, e.g., at the Γ point for the high-energy polaritonic branches (orange solid lines), and along the low-energy branches for intermediate momenta (green solid lines)]. Since these special points with zero derivative lie on high-symmetry axes, it suggests the existence of polaritonic states with vanishing group velocity. These may open interesting perspectives for stopping and storing light in our proposed cubic metacrystals.

The experimental observability of the band gaps and of their modulation discussed above may be hindered by damping mechanisms leading to the decay of the plasmon polaritons. The latter are mostly subject to two sources of damping: Ohmic (absorption) losses with decay rate γ^a inherent to any type of metallic nanostructure, and Landau damping with

decay rate γ^L , i.e., the decay of the plasmon excitation into electron-hole pairs [28, 29]. Note that radiation damping is irrelevant for the infinite metacrystals considered here due to the very nature of a plasmon polariton as a coherent superposition of plasmonic and photonic fields. Absorption losses were experimentally estimated to be of the order of $\hbar\gamma^a \simeq 70$ meV for Ag nanoparticles [30]. Moreover, it has been shown that Landau damping only weakly depends on the dipole-dipole interaction [31], so that we estimate it with the Landau damping of a single nanoparticle. This yields $\gamma^L = 3v_F g/4r$, where v_F is the Fermi velocity and g is a numerical factor of the order of 1 [28, 29, 32, 33]. For Ag nanoparticles, we obtain $\hbar\gamma^L \simeq 690$ meV/ r [nm]. For the nanoparticle radii that we consider (typically of the order of 10 nm), the total linewidth of the plasmon polariton band structure is therefore of the order of 140 meV. For this reason the gaps in the plasmon polariton dispersion, as well as their polarization dependence for certain directions in the first Brillouin zone should be clearly accessible.

IV. CONCLUSIONS

We have considered in this work plasmon polaritons in sc, fcc and bcc lattices of spherical metallic nanoparticles. We have developed a quantum model, justified for small nanoparticles (i.e., with a radius in between ca. 1 nm and 20 nm), where quantum size-effects such as Landau damping are significant. The near-field dipole-dipole interaction between the nanoparticles leads to collective plasmons which are delocalized over the metacrystal. The strong coupling of these collective plasmons to photons results in the formation of plasmon polaritons.

Our model enabled us to obtain semi-analytical expressions

which determine both the collective plasmon dispersions and their corresponding polarizations, as well as the plasmon polariton dispersions, which we have analyzed in detail for the three cubic lattices. In particular, we have shown that the polaritonic dispersion presents band gaps in the near-infrared to the visible range of the spectrum for all three cubic lattices and for all high-symmetry axes starting from the center of the first Brillouin zone. Remarkably, for special directions in the reciprocal space, the polaritonic gap depends on the plasmon polarization, suggesting the possibility to realize a birefringent metacrystal, despite the high degree of cubic symmetry of the latter. Moreover, plasmon polariton states are found to present a vanishing group velocity, opening up interesting perspectives for stopping and storing light in metallic nanoparticle-based plasmonic metamaterials.

ACKNOWLEDGMENTS

We thank P. Gilliot for enlightning discussions and C. A. Downing for his careful reading of the manuscript. SL, FH and FP acknowledge funding through the Junior Professorship Program of the Ministry of Science, Research and the Arts (MWK) of Baden-Württemberg on “Theory of Plasmonic Nanostructures”, the Carl Zeiss Foundation, and the Center for Applied Photonics (CAP). EM acknowledges financial support of the Royal Society (International Exchange Grant No. IE140367) and of the Leverhulme Trust (Research Project Grant RPG-2015-101). GW is grateful to the French National Research Agency ANR (Project Nr. ANR-14-CE26-0005 Q-MetaMat) and the CNRS PICS program (Contract Nr. 6384 APAG) for financial support. Part of this work was performed on the computational resource bwUniCluster, funded by MWK and the Universities of the State of Baden-Württemberg within the framework program bwHPC.

-
- [1] W. L. Barnes, A. Dereux, and T. W. Ebbesen, “Surface plasmon subwavelength optics,” *Nature* **424**, 824 (2003).
 - [2] S. A. Maier, *Plasmonics: Fundamentals and Applications* (Springer Berlin, Heidelberg, 2007).
 - [3] N. J. Halas, S. Lal, W.-S. Chang, S. Link, and P. Nordlander, “Plasmons in strongly coupled metallic nanostructures,” *Chem. Rev.* **111**, 3913 (2011).
 - [4] N. Meinzer, W. L. Barnes, and I. R. Hooper, “Plasmonic meta-atoms and metasurfaces,” *Nature Photon.* **8**, 889 (2014).
 - [5] V. M. Shalaev, “Transforming light,” *Science* **322**, 384 (2008).
 - [6] M. S. Tame, K. R. McEnery, S. K. Ozdemir, J. Lee, S. A. Maier, and M. S. Kim, “Quantum plasmonics,” *Nature Phys.* **9**, 329 (2013).
 - [7] M. B. Ross, C. A. Mirkin, and G. C. Schatz, “Optical properties of one-, two-, and three-dimensional arrays of plasmonic nanostructures,” *J. Phys. Chem. C* **120**, 816 (2015).
 - [8] S. J. Tan, M. J. Campolongo, D. Luo, and W. Cheng, “Building plasmonic nanostructures with DNA,” *Nature Nanotech.* **6**, 268 (2011).
 - [9] Y. Kim, R. J. Macfarlane, M. R. Jones, and C. A. Mirkin, “Transmutable nanoparticles with reconfigurable surface ligands,” *Science* **351**, 579 (2016).
 - [10] W. Liu, M. Tagawa, H. L. Xin, T. Wang, H. Emamy, H. Li, K. G. Yager, F. W. Starr, A. V. Tkachenko, and O. Gang, “Diamond family of nanoparticle superlattices,” *Science* **351**, 582 (2016).
 - [11] M. Quinten, A. Leitner, J. R. Krenn, and F. R. Aussenegg, “Electromagnetic energy transport via linear chains of silver nanoparticles,” *Opt. Lett.* **23**, 1331 (1998).
 - [12] M. L. Brongersma, J. W. Hartman, and H. A. Atwater, “Electromagnetic energy transfer and switching in nanoparticle chain arrays below the diffraction limit,” *Phys. Rev. B* **62**, R16356 (2000).
 - [13] S. A. Maier, P. G. Kik, and H. A. Atwater, “Optical pulse propagation in metal nanoparticle chain waveguides,” *Phys. Rev. B* **67**, 205402 (2003).
 - [14] S. Y. Park and D. Stroud, “Surface-plasmon dispersion relations in chains of metallic nanoparticles: An exact quasistatic calculation,” *Phys. Rev. B* **69**, 125418 (2004).
 - [15] W. H. Weber and G. W. Ford, “Propagation of optical excitations by dipolar interactions in metal nanoparticle chains,” *Phys. Rev. B* **70**, 125429 (2004).
 - [16] D. S. Citrin, “Coherent excitation transport in metal-

- nanoparticle chains,” *Nano Lett.* **4**, 1561 (2004).
- [17] D. S. Citrin, “Plasmon-polariton transport in metal-nanoparticle chains embedded in a gain medium,” *Opt. Lett.* **31**, 98 (2006).
 - [18] A. F. Koenderink and A. Polman, “Complex response and polariton-like dispersion splitting in periodic metal nanoparticle chains,” *Phys. Rev. B* **74**, 033402 (2006).
 - [19] V. A. Markel and A. K. Sarychev, “Propagation of surface plasmons in ordered and disordered chains of metal nanospheres,” *Phys. Rev. B* **75**, 085426 (2007).
 - [20] A. F. Koenderink, “Plasmon nanoparticle array waveguides for single photon and single plasmon sources,” *Nano Lett.* **9**, 4228 (2009).
 - [21] M. Petrov, “Disorder-induced Purcell enhancement in nanoparticle chains,” *Phys. Rev. A* **91**, 023821 (2015).
 - [22] C. Lee, M. Tame, J. Lim, and J. Lee, “Quantum plasmonics with a metal nanoparticle array,” *Phys. Rev. A* **85**, 063823 (2012).
 - [23] G. Weick, C. Woollacott, W. L. Barnes, O. Hess, and E. Mariani, “Dirac-like plasmons in honeycomb lattices of metallic nanoparticles,” *Phys. Rev. Lett.* **110**, 106801 (2013).
 - [24] T. J. Sturges, C. Woollacott, G. Weick, and E. Mariani, “Dirac plasmons in bipartite lattices of metallic nanoparticles,” *2D Mater.* **2**, 014008 (2015).
 - [25] G. Weick and E. Mariani, “Tunable plasmon polaritons in arrays of interacting metallic nanoparticles,” *Eur. Phys. J. B* **88**, 7 (2015).
 - [26] J. J. Hopfield, “Theory of the contribution of excitons to the complex dielectric constant of crystals,” *Phys. Rev.* **112**, 1555 (1958).
 - [27] J. F. Nye, *Physical Properties of Crystals* (Oxford University Press, Oxford, 1985) p. 329.
 - [28] U. Kreibig and M. Vollmer, *Optical Properties of Metal Clusters* (Springer, Berlin, 1995).
 - [29] A. Kawabata and R. Kubo, “Electronic properties of fine metallic particles - II. Plasma resonance absorption,” *J. Phys. Soc. Jpn.* **21**, 1765 (1966).
 - [30] K.-P. Charlé, W. Schulze, and B. Winter, “The size dependent shift of the surface plasmon absorption band of small spherical metal particles,” *Z. Phys. D* **12**, 471 (1989).
 - [31] A. Brandstetter-Kunc, G. Weick, D. Weinmann, and R. A. Jalabert, “Decay of dark and bright plasmonic modes in a metallic nanoparticle dimer,” *Phys. Rev. B* **91**, 035431 (2015).
 - [32] C. Yannouleas and R. A. Broglia, “Landau damping and wall dissipation in large metal clusters,” *Ann. Phys. (NY)* **217**, 105 (1992).
 - [33] G. Weick, R. A. Molina, D. Weinmann, and R. A. Jalabert, “Lifetime of the first and second collective excitations in metallic nanoparticles,” *Phys. Rev. B* **72**, 115410 (2005).